ELSEVIER

Journal of Fluids and Structures 20 (2005) 519–531

JOURNAL OF FLUIDS AND STRUCTURES

www.elsevier.com/locate/jfs

DNS of flow past a stationary and oscillating cylinder at Re = 10 000

S. Dong, G.E. Karniadakis*

Division of Applied Mathematics, Center for Fluid Mechanics, Brown University, Box 1966, 37 Manning Street, Providence, RI 02912, USA

Received 10 September 2004; accepted 19 February 2005

Abstract

Results of direct numerical simulations (DNS) are presented for turbulent flows past a stationary circular cylinder and past a rigid cylinder undergoing forced harmonic oscillations at Reynolds number Re = 10 000. This significant increase in Reynolds number (compared to previous DNS) is accomplished by employing a multilevel-type parallel algorithm within the spectral element framework. Comparisons with the available experimental data show that the simulation has captured the flow physical quantities and the statistics of the cylinder wake correctly.

Keywords: Flow structure interaction; Vortex induced vibration; Cylinder flow; High Reynolds number flow; Spectral element method

1. Introduction

Turbulent flow past a circular cylinder has been the subject of a large volume of experimental and numerical investigations [see Williamson (1996), Williamson and Govardhan (2004), Sarpkaya (2004) and references therein]. For regimes at low Reynolds numbers, below a few hundred, a good understanding of the physics has been obtained in recent years (Triantafyllou et al., 2004). At higher (but still subcritical) Reynolds numbers, however, considerably less is known. Recent efforts at higher Reynolds numbers (mostly experimental work) have focused on the shear layer instability (Unal and Rockwell, 1988) and the scaling of the shear layer frequency with respect to the Reynolds number (Prasad and Williamson, 1997). At these Reynolds numbers, there are also indications of those phenomena observed at low Reynolds numbers, such as oblique shedding modes, cellular shedding and vortex dislocations (Norberg, 1992; Szepessy and Bearman, 1992; Prasad and Williamson, 1997). However, many important questions remain unanswered such as the extent of the 3-D vortex dynamics phenomena observed at low Reynolds numbers that can carry over to high Reynolds numbers and their influence on the unsteady fluid forces on the cylinder.

1.1. Stationary cylinder

Numerical simulations of the cylinder flow, though largely confined to 2-D or 3-D flows at very low Reynolds numbers, have provided insight into the flow instability and the vortex dynamics in the cylinder wake (Henderson,

*Corresponding author. Tel.: +1 401 863 1217; fax: +1 401 863 3369.
E-mail address: gk@dam.brown.edu (G.E. Karniadakis).

0889-9746/$ - see front matter
doi:10.1016/j.jfluidstructs.2005.02.004

1997). In recent years, a number of simulations at higher Reynolds numbers, $Re = 10^3$–10^6 (Travin et al., 1999; Catalano et al., 2003), mostly large eddy simulations (LES), have been carried out thanks to the significant and steady increase in the computing power. Due to the overwhelming volume of literature on this topic, in the following review we restrict ourselves to the cylinder flow simulations at Reynolds numbers higher than about 500.

The cylinder flow at Reynolds number $Re = 3900$ has become a canonical test case for LES. Beaudan and Moin (1994), Mittal and Moin (1997), Kravchenko and Moin (1998) are among the first to undertake LES studies at this Reynolds number. The mean velocity and Reynolds stress profiles from these three simulations are in good agreement with the experimental data far downstream. However, several issues exist regarding the power spectra and the mean velocity in the recirculation region. The significant numerical dissipation in the upwind scheme in Beaudan and Moin (1994) results in overdamping in the velocity power spectra at high wavenumbers. This is better controlled in Mittal and Moin (1997) by using a central finite-difference scheme. The power spectra show more energetic turbulence scales than those in the upwind scheme, and the simulated spectra are in agreement with the experimental data over a wider range of wavenumbers. On the other hand, no clear inertial range is obtained in either of these two simulations. The inertial range is accurately captured in Kravchenko and Moin (2000), who employ a high-order method based on B-spline and zonal grids. Although the mean velocity profiles from all three simulations agree with one another, in the vicinity of the cylinder they all differ from the experimental velocity profile in shape. Several other researchers have examined a variety of aspects that affect the quality of LES of the cylinder flow at $Re = 3900$. The numerical and modeling aspects are investigated by Breuer (1998), who employs five different numerical schemes and two subgrid-scale models in LES. Central difference schemes are observed to yield results in better agreement with the experimental data than dissipative methods, and low-order upwind schemes are observed to fail to predict several important physical quantities correctly. The effect of the averaging time on the accuracy of statistical quantities in LES is studied by Franke and Frank (2002), who observed a notable influence on the values of the base pressure coefficient and the recirculation bubble length by the accumulation time. Jordan (2003) has studied the effect of high-order compact and explicit upwind differencing schemes together with four different forms of convective derivatives for the cylinder flow at $Re = 3900$. He concludes that it is important to resolve the inertial range in LES as the upwind scheme coupled with dynamic subgrid-scale model lacks full control over the aliasing when the wavenumber cutoff falls within the lower limit of the inertial range.

A direct numerical simulation (DNS) of the cylinder flow at $Re = 3900$ is performed by Ma et al. (2000), who employ a Fourier expansion and a spectral element discretization on unstructured mesh in the spanwise direction and streamwise-crossflow planes, respectively. The mean velocity profiles and the power spectra are in good agreement with the experimental data in the near wake as well as far downstream. In particular, the mean velocity profiles agree well with those from experiments in the vicinity of the cylinder. Compared with LES (Kravchenko and Moin, 2000), the base pressure coefficient in DNS is a little lower, while the recirculation bubble length is larger. Franke and Frank (2002) find that this is an effect of the averaging time in computing statistics. In DNS (Ma et al., 2000) the statistics is accumulated over 600 convective time units (D/U_0), while in LES (Kravchenko and Moin, 2000) the statistics is accumulated over about 35 convective time units. Franke and Frank (2002) observe that as the averaging time increases, the values of the base pressure coefficients and recirculation bubble length start from those in Kravchenko and Moin (2000) and gradually change to those in Ma et al. (2000).

The cylinder flow at higher Reynolds numbers has been considered in several LES studies in the past few years. Jordan (2002) studied the shear layer instability at $Re = 8000$ using an upwind finite difference scheme and dynamic subgrid-scale model. The simulation has captured several parameters correctly. However, the lift coefficient is much lower than the experimental consensus (Norberg, 2003). In addition, the short time history collected (about 25 convective units) compromises the reliability of the power spectra and the accuracy of the Strouhal frequency. Another LES study was conducted by Kalro and Tezduyar (1997) for cylinder flow at $Re = 10\,000$ using a stabilized finite element formulation and a Smagorinsky subgrid-scale model. The predicted drag coefficient and Strouhal number are in fair agreement with the experimental data. However, no grid refinement was conducted and no statistics was reported. Breuer (2000) investigated the cylinder flow at Reynolds number $Re = 140\,000$ in order to evaluate the applicability of LES to practical high Reynolds number flows. The predicted integral parameters and the mean velocity profiles are in reasonable agreement with the experimental data. A questionable result in this study is that the grid refinement does not lead to improved results in terms of the agreement with the experimental data. Still higher Reynolds numbers (supercritical) from $Re = 5 \times 10^5$ to 2×10^6 have been attempted recently by Catalano et al. (2003) using LES and a wall model. The mean pressure distribution is predicted reasonably well at lower Reynolds numbers, while the results are inaccurate at the higher end of Reynolds number.

Several DNS of the cylinder flow have been reported in literature with $Re > 500$. Except for Ma et al. (2000) at $Re = 3900$, which is the highest Reynolds number DNS has achieved, other DNS studies are performed at much lower Reynolds numbers. With a series of careful DNS studies for Reynolds numbers ranging from 10 to 1000, Henderson (1997) has significantly improved our understanding of the flow transition from 2-D to 3-D states. It is demonstrated that three-dimensionality in the wake leads to irregular states and fast transitions to turbulence at Reynolds numbers

just beyond the onset of the secondary instability. The three-dimensionality effect on the accuracy of simulations has been investigated by Batcho and Karniadakis (1991) at Re = 500 and Mittal and Balachandar (1995) at Re = 525 through a number of 2-D and 3-D DNS. It is found that the overprediction of fluid forces in 2-D simulations is primarily an intrinsic 3-D effect. This point is exemplified in the 2-D direct simulations at Reynolds numbers ranging from Re = 100 to 10 000 (Braza et al., 1986, 1990; Mittal and Kumar, 2001).

1.2. Cylinder subject to vortex induced vibrations (VIV)

Sarpkaya (2004) and Williamson and Govardhan (2004) provide a comprehensive overview of the field of vortex-induced vibrations (VIV) regarding the progress, current state and debate, and the numerous unresolved problems. Here we concentrate on the review of numerical simulations of VIV of a circular cylinder with Reynolds numbers higher than about 500.

While a number of 2-D VIV simulations are reported in the literature, the number of 3-D numerical studies is quite limited. Blackburn et al. (2000) combine DNS and a PIV experiment to study the flow past a freely vibrating cylinder at Re = 556, and demonstrate the significance of three-dimensionality in numerical simulations in order to capture the structural response correctly. They show that 2-D simulations are inadequate in predicting the response envelope and the vortex shedding mechanics, and that 3-D simulations are required to reproduce the experimental observations. These findings on the 3-D effect are in accordance with those for the stationary cylinder situations (Batcho and Karniadakis, 1991; Mittal and Balachandar, 1995). The vortex dynamics and flow structures in the turbulent wake of rigid and flexible cylinders subject to VIV are studied in detail by Evangelinos and Karniadakis (1999) and Evangelinos et al. (2000) using spectral DNS at Re = 1000. The structural response amplitude is observed to be on the order of one cylinder diameter, significantly higher than that in laminar wakes. They observe two types of oscillations, corresponding to traveling and standing wave responses, respectively. The latter produces a slightly larger oscillation amplitude. Lucor et al. (2001) considered VIV of very long flexible cylinders (with aspect ratio >500) under sheared approach flow for Re = 1000. It is observed that, with a linear shear approach flow profile, the structural response resembles a standing-wave pattern, while with an exponential shear in-flow profile it resembles a mixed standing-traveling wave pattern. Tutar and Holdo (2000) conducted an LES (2-D and 3-D) of the flow past a forced oscillating cylinder at Re = 24 000 using the Smagorinsky model and a damping term in the cylinder boundary layer. While the Strouhal number is in fair agreement with experimental data, large discrepancy in the pressure coefficient is observed. The 3-D simulation result is observed to agree better with experimental result. More recently, a quasi 3-D LES using strip theory is conducted for VIV of a long flexible pipe at $Re = 2.84 \times 10^5$ (Willden and Graham, 2004). The flow is computed on a number of locations along the spanwise direction. At each spanwise location, the flow is assumed to be 2-D and the 2-D Navier–Stokes equations are solved. A multimodal response of the structure is observed from the simulation, qualitatively similar to the full DNS of Lucor et al. (2001).

Despite their inherent limitations at high Reynolds numbers (Mittal and Balachander, 1995; Blackburn et al., 2000; Tutar and Holdo, 2000), 2-D simulations have been widely applied to high Reynolds number VIV studies. Blackburn and Henderson (1999) report 2-D DNS results of the flow past a forced oscillating cylinder at Re = 500. It is demonstrated that the phase switch in vortex shedding results from the competition of two vorticity production mechanisms, namely by the tangential pressure gradient on the cylinder surface and by the surface-tangential component of cylinder acceleration. Skaugset and Larson (2003) combine 2-D DNS at Re = 800 and experiment to examine the suppression of VIV, and demonstrate that steady blowing of radial water jets along the cylinder effectively reduces VIV amplitudes. Dalton and collaborators (Lu and Dalton, 1996; Zhang and Dalton, 1996; Al-Jamal and Dalton, 2004) have conducted extensive 2-D LES of VIV at Reynolds numbers from Re = 185 to 13 000, and found qualitative agreement with experimental results. Mittal and Kumar (2001) conducted a 2-D VIV simulation of a circular cylinder at Reynolds numbers from Re = 1000 to 10 000 using a stabilized space-time finite element approach. The drag and lift coefficients are observed to be significantly overpredicted, similar to the findings by previous researchers (Mittal and Balachandar, 1995).

1.3. Objective

The present study focuses on the cylinder flow at Re = 10 000. We have pursued 3-D DNS of the turbulent flow past a stationary cylinder as well as past a rigid cylinder undergoing forced harmonic oscillations in the cross-flow direction. The reason for choosing this Reynolds number is manifold. An important consideration is the availability of the experimental data (Gopalkrishnan, 1993; Saelim and Rockwell, 2003). This Reynolds number is about one order of magnitude higher than the one considered in previous DNS of VIV (Evangelinos and Karniadakis, 1999) and is about 2.5 times the one in previous DNS of stationary cylinder flow (Ma et al., 2000), thus allowing for a more "mature"

turbulent wake (i.e., exhibiting a larger inertial subrange) than in previous simulations. The computational cost associated with this significant increase in Reynolds number is tackled by employing an efficient multilevel-type parallel algorithm in the computations.

We employ a spectral/*hp* element discretization on unstructured grids in streamwise-crossflow planes and a Fourier spectral expansion in the spanwise direction. A third-order accurate stiffly stable pressure correction-type scheme is employed for time integration (Karniadakis et al., 1991). We have conducted extensive grid refinement tests, and compared the flow integral parameters and statistical quantities with the available experimental data. The focus of this paper is on the comparison with experiments to evaluate these first simulation results.

2. Parallel computation issues

Realistic simulations of flow past a cylinder subject to VIV at high Reynolds numbers require high resolution in the streamwise and cross-flow directions and a large number of Fourier modes along the cylinder span. Careful analysis indicates that VIV computations demonstrate inherent hierarchical structures when the problem is discretized with spectral/*hp* element methods (Karniadakis and Sherwin, 1999). Consider an incompressible flow past a cylinder subject to VIV. We assume the flow and cylinder variables are periodic in the homogeneous direction. A combined spectral-element/Fourier-discretization can be employed to accommodate the requirement of high order, as well as efficient handling of complex computational domain in the nonhomogeneous planes. Spectral expansions in the homogeneous direction employ Fourier modes that are decoupled except in the nonlinear terms. Each Fourier mode is a 2-D field and solved with the spectral element approach. Computations on the Fourier modes, spectral element plane, spectral elements within the plane, and at the subelement level form the hierarchy of operations in the solution process of the VIV problem. Multilevel parallelism naturally suits such VIV computations with inherent hierarchical structures (Dong and Karniadakis, 2004a).

To exploit the inherent hierarchical structures in the computations, we employ an MPI/MPI two-level parallel algorithm (Dong and Karniadakis, 2004b) for simulating the cylinder flow at $Re = 10\,000$. Specifically, the flow domain is first decomposed along the cylinder span. Each subdomain consists of one or more Fourier modes in the Fourier space. At the first level are groups of MPI processes, with each group computing one subdomain. The spectral element mesh in the nonhomogeneous planes are partitioned using a graph-partitioning algorithm (Karypis and Kumar, 1998) at the second level. Each subdomain at the second level comprises structured or unstructured elements. Accordingly, each MPI process within the group computes a sub-domain at the second level. The key advantage of this parallel algorithm is that MPI processes participate in communications at different levels and communicate only with the other processes at the same level. As a result, compared with a single-level computation on the same number of processors, much fewer processes are involved in each communication. This reduces the communication latency overhead and enables the applications to scale to a large number of processors more efficiently. This is demonstrated by the performance result in Table 1 for up to 1536 processors obtained on a Compaq Alpha cluster for the cylinder flow at $Re = 10\,000$ with a problem size of 300 000 000 degrees of freedom.

3. Flow configuration and parameters

We consider the incompressible turbulent flow past a rigid circular cylinder with two configurations: (i) a stationary cylinder, and (ii) a rigid cylinder undergoing a forced harmonic oscillation in the cross-flow direction. Following

Table 1
Performance of MPI/MPI parallel algorithm for cylinder flow at $Re = 10\,000$ with a problem size of 300 000 000 degrees of freedom on a Compaq Alpha cluster (1 GHz Alpha CPU)

CPU	Seconds/step	Speed-up(×256)	Efficiency
256	14.766	1.0	1.0
512	7.417	1.991	0.996
1024	3.882	3.804	0.951
1536	2.877	5.132	0.856

Parallel speed-up is computed based on the wall time on 256 processors. Efficiency is defined as the parallel speed-up divided by the number of processors. (The number of processors needs to be divided by 256 here since speed-up is calculated based on the time on 256 processors.)

Newman and Karniadakis (1997), we solve the Navier–Stokes equations in a coordinate system attached to the cylinder, which avoids the difficulty of a moving mesh in the oscillating-cylinder case. For time integration, we employ a stiffly-stable pressure correction-type scheme (Karniadakis et al., 1991) with a third-order accuracy in time. For spatial discretizations, we employ a Fourier spectral expansion in the homogeneous direction and a spectral element approach (Karniadakis and Sherwin, 1999) in the streamwise and cross-flow directions.

We focus on the turbulent wake at Reynolds number $\mathrm{Re} = 10\,000$ based on the in-flow velocity and the cylinder diameter. For the moving cylinder case, the cylinder oscillation in the cross-flow (y) direction is expressed by

$$y = Y_0 \cos(2\pi f_0 t), \tag{1}$$

where y is the cylinder displacement at time t, Y_0 is the cylinder displacement amplitude, and f_0 is the cylinder oscillation frequency. All length variables are normalized with the cylinder diameter D.

The computational domain extends from $-20D$ at the inlet to $50D$ at the outlet, and from $-20D$ to $20D$ in the cross-flow direction. The spanwise dimension of the domain L_z is chosen to be $L_z/D = \pi$. A "z-slice" of the computational domain is shown in Fig. 1. We conducted simulations on two spectral element meshes in each x–y plane: a coarser mesh consisting of $K = 6272$ triangular elements (Fig. 1(a)) and a mesh significantly refined around and in the near-wake of the cylinder that consists of $K = 9272$ triangular elements (Fig. 1(b)). The order per element is varied between $P = 4$ and $P = 5$. Fig. 1(c) shows the mean streamwise velocity profile along a vertical line crossing the cylinder axis. It indicates that, within the cylinder boundary layer, we have over one layer of spectral elements or more than six grid points with the coarser mesh (Fig. 1(a)), and over two layers of spectral elements or more than 12 grid points with the finer mesh (Fig. 1(b)).

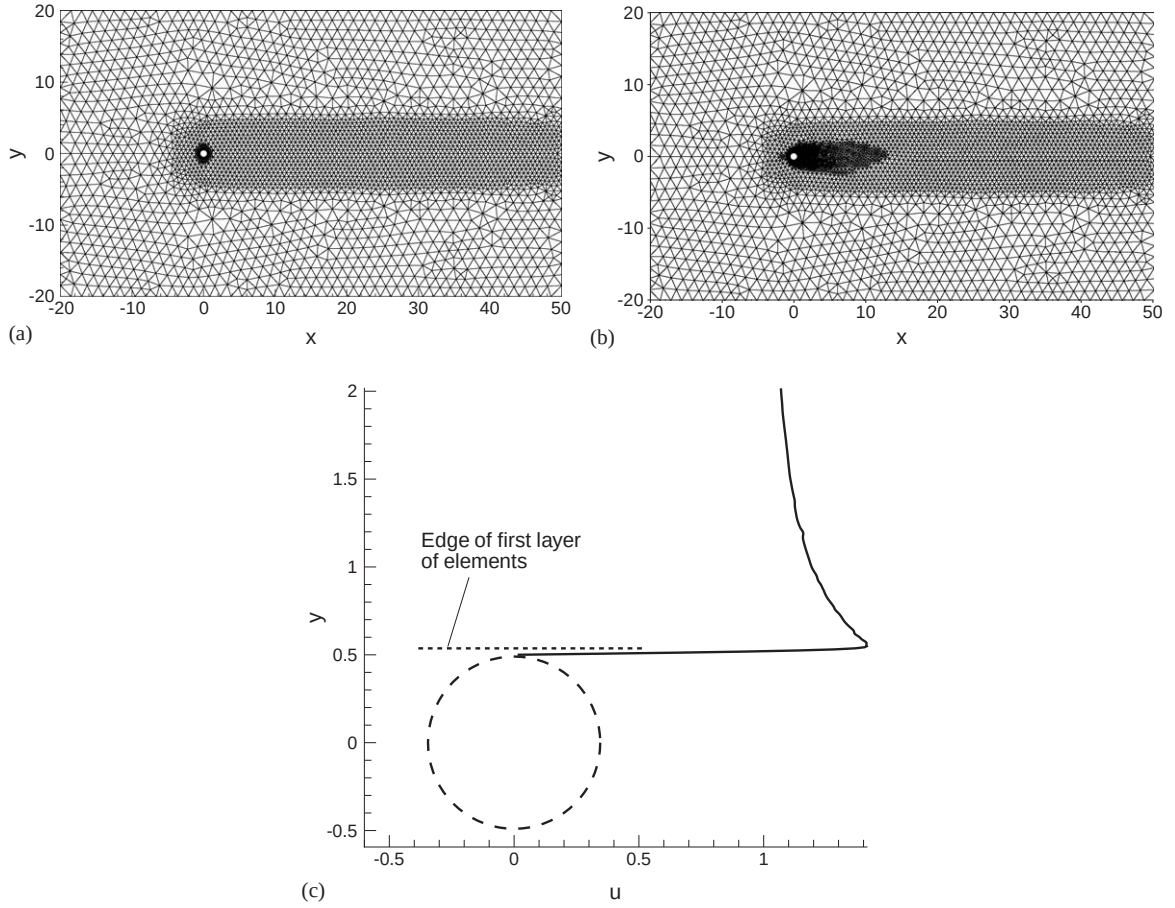

Fig. 1. 2-D slice of mesh in x–y planes (spanwise dimension of domain $L_z/D = \pi$) and resolutions: (a) low-resolution mesh consisting of 6272 triangular spectral elements; (b) high-resolution mesh consisting of 9272 triangular spectral elements; (c) mean streamwise velocity profile along a vertical line crossing the cylinder.

Table 2
Physical quantities in the flow past a stationary cylinder at Re = 10 000: drag coefficient C_d, base pressure coefficient C_{p_b}, Strouhal number St, and r.m.s. lift coefficient C_L

Cases	C_d	$-C_{p_b}$	St	C_L
DNS-A1 ($P = 5$, $N_z = 16$, $K = 6272$)	1.155	1.129	0.195	0.538
DNS-A2 ($P = 5$, $N_z = 64$, $K = 6272$)	1.110	1.084	0.209	0.565
DNS-A3 ($P = 5$, $N_z = 128$, $K = 6272$)	1.128	1.171	0.205	0.574
DNS-B1 ($P = 5$, $N_z = 32$, $K = 9272$)	1.208	1.201	0.200	0.547
DNS-B2 ($P = 4$, $N_z = 64$, $K = 9272$)	1.120	1.056	0.205	0.497
DNS-B3 ($P = 5$, $N_z = 128$, $K = 9272$)	1.143	1.129	0.203	0.448
Wieselsberger (1921)	1.143	—	—	—
Bishop and Hassan (1964)	—	—	0.201	0.463
Moeller and Leehey (1984)	—	—	—	0.532
Gopalkrishnan (1993)	1.186	—	0.193	0.384
West and Apelt (1993)	—	—	—	0.461
Williamson (1996)	—	1.112	—	—
Norberg (2003)	—	—	0.202	0.394

The order of spectral elements is denoted by P; N_z is the number of grid points in the spanwise z-direction; K denotes the number of spectral elements in x–y planes.

Simulations were performed with different grid resolutions by varying the number of grid points (or Fourier modes) in the spanwise z-direction and the order of spectral elements in the x–y planes on the two spectral element meshes. Table 2 summarizes the values of several physical quantities under a number of resolutions from the simulation together with their experimental values for the flow past a stationary cylinder at Re = 10 000. The CPU time required for each case ranges from about 20 000 h to about 250 000 h as the resolution increases. The drag coefficients, base pressure (base suction) coefficients, and the Strouhal number from the simulation are in quite good agreement with the experimental data for all resolutions, indicating that these physical quantities are generally not too sensitive to the grid resolution. On the other hand, the lift coefficient (based on r.m.s. lift) demonstrates a higher sensitivity to the resolution. With the low-resolution mesh, the values of the lift coefficient from the simulation lie generally at the upper bound of the range of experimental lift coefficient data, and the value increases slightly as the number of Fourier modes in the spanwise direction increases. With the high-resolution mesh, the values of the lift coefficient decrease as the number of Fourier modes in the spanwise direction increases, and fall within the range of experimentally measured values. It is noted that the lift coefficient demonstrates a wide spread in the experiments, and large differences about the lift coefficient values exist among different experiments. Even from the same experiment, the lift coefficient values show a large scatter from one run to another. Gopalkrishnan (1993) shows that the standard deviation of his lift coefficient data is 0.087 and the actual lift coefficient values realized in his measurements range from 0.2 to 0.55. Norberg (2003) provides an empirical formula for the lift coefficient by considering the reported values from a number of experiments:

$$C_L = 0.52 - 0.06x^{-2.6}, \quad x = \log_{10}\frac{\mathrm{Re}}{1600}, \quad 5400 \leqslant \mathrm{Re} \leqslant 220\,000.$$

At Re = 10 000, this formula gives a lift coefficient of 0.411, which is about in the middle between the computed value in case DNS-B3 ($C_L = 0.448$) and Norberg's ($C_L = 0.394$) and Gopalkrishnan's ($C_L = 0.384$) reported values.

4. Results and discussion

We present simulation results of the cylinder flow at Re = 10 000 under the two configurations described in the previous section. Our emphasis is on comparisons with the experimental data. We will compare the flow statistics of the cylinder wake between the simulation and PIV experiment for the stationary case (Saelim and Rockwell, 2003), and compare several physical quantities between the simulation and the experiment by Gopalkrishnan (1993) for the oscillation case.

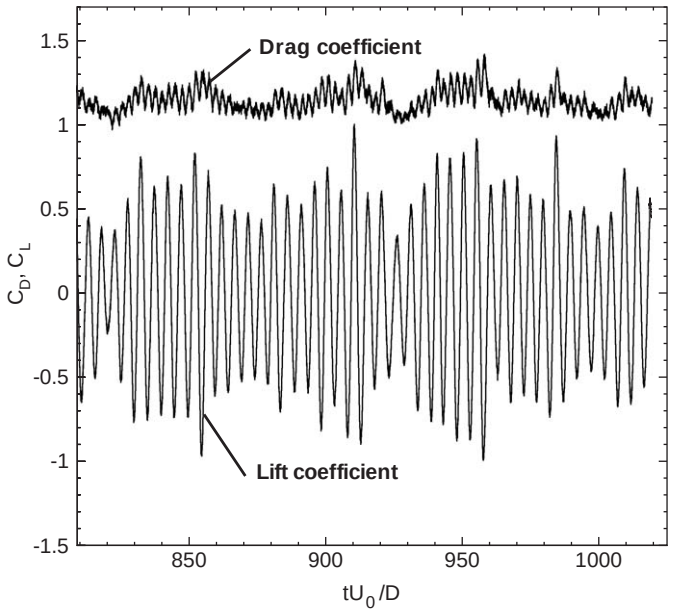

Fig. 2. Time history of drag coefficient and lift coefficient of the flow past a stationary cylinder at Re = 10 000 (Case DNS-B3).

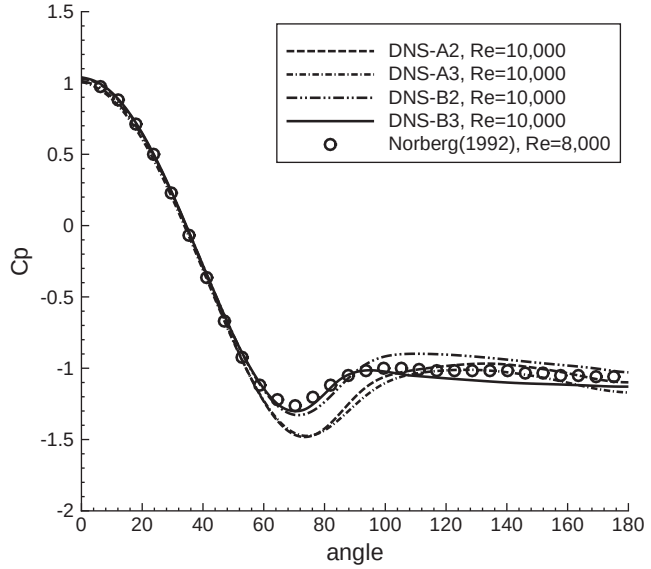

Fig. 3. Comparison of pressure coefficients on cylinder surface between simulation (Re = 10 000) and experimental data (Re = 8000) in Norberg (1992).

4.1. *Turbulent flow past a stationary cylinder at* Re = 10 000

To obtain the DNS results presented here, the simulations have advanced more than 1000 convective time units (D/U_0, where U_0 is the inflow velocity). The nondimensional time step typically lies between 2.5×10^{-4} and 5.0×10^{-4}. Fig. 2 shows a window of the time history of the drag and lift coefficients for the case $P = 5$, $N_z = 128$, and $K = 9272$. The time traces reveal the quasi-periodic behavior of drag and lift coefficients, with their amplitudes varying irregularly

over time. The drag coefficients and the lift coefficients from this and the other cases are listed in Table 2. They are in good agreement with the experimental data at $Re = 10\,000$.

We first examine the mean pressure distribution on the cylinder surface. In Fig. 3 we plot the cylinder surface pressure coefficients as a function of the angle, with zero degree of the angle located at the front stagnation point. The figure shows results on both the low- and high-resolution meshes at $Re = 10\,000$ from the simulation, together with the experimental data by Norberg (1992) at $Re = 8000$. The low-resolution mesh seems to capture the pressure on the front (angle $<60^\circ$) and the back (angle $>100^\circ$) portions of the cylinder surface reasonably well. However, this mesh overpredicts the magnitude of the minimum pressure on the cylinder surface and the angle at which the minimum occurs. The results from the high-resolution mesh, on the other hand, show much better agreement with the experimental result. With the highest resolution (case DNS-B3) the result agrees with the experimental data reasonably well on the entire cylinder surface.

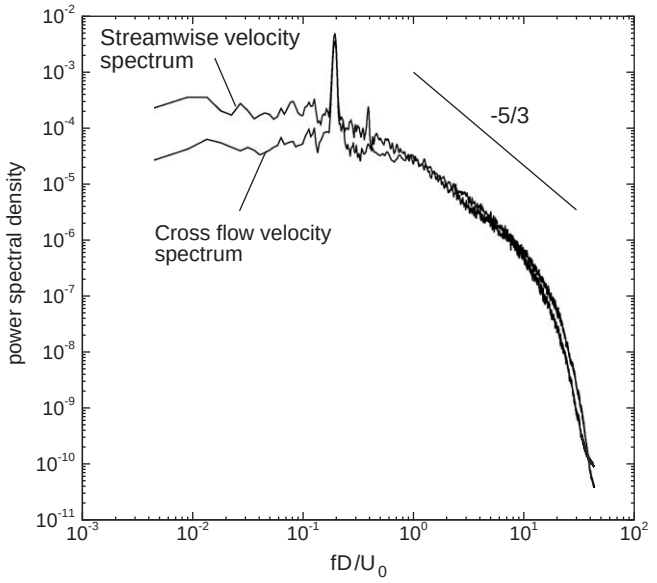

Fig. 4. Spectra of streamwise and cross-flow velocities at point $x = 1.12$, $y = 0.8$ in the wake of a stationary cylinder at $Re = 10\,000$.

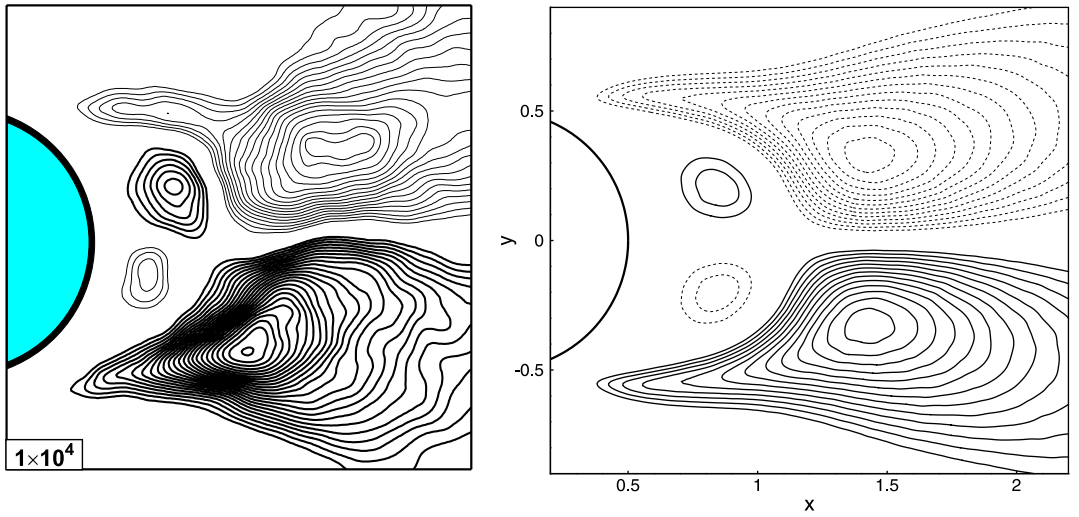

Fig. 5. Comparison of the Reynolds stress $\langle u'v' \rangle$ between PIV experiment (Saelim and Rockwell, 2003) (left) and current simulations (right). Contours of the experimental data and the simulation results are plotted on the same levels: $|\langle u'v' \rangle|_{\min} = 0.03$ and $\Delta\langle u'v' \rangle = 0.01$. Dashed lines denote negative values.

In Fig. 4 we show the power spectra of the streamwise and cross-flow velocities, at a point $x = 1.12$ and $y = 0.8$ off the centerline in the cylinder wake, as a function of the nondimensional frequency. The sharp peak in the spectra marks the Strouhal frequency. A second weaker peak is also visible in the streamwise velocity spectrum. The streamwise velocity spectrum and the crossflow velocity spectrum essentially coincide with each other in the inertial subrange, which follows a $-5/3$ power-law scaling (Fig. 4). The initial subrange covers about a decade in frequency at this Reynolds number.

Flow statistics (mean, r.m.s. velocities and Reynolds stress) are computed by averaging the flow variables temporally, and also spatially along the homogeneous z-direction. The statistical quantities are accumulated over a long period of time to ensure their convergence. This typically amounts to over 200 convective times units (or more than 40 shedding cycles or over three "flow-through" times, L_x/U_0, where L_x is the streamwise dimension of flow domain). We have compared the mean flow, r.m.s. velocities and the Reynolds stress from the simulation with the PIV experimental data by Saelim and Rockwell (2003) at the same Reynolds number, and observed a good agreement between the simulation results and the experimental measurement. In Fig. 5 we plot contours of the Reynolds stress $\langle u'v' \rangle$, where u' and v' are streamwise and crossflow r.m.s. velocities, respectively, from the PIV experiment (left plot) and from current simulation (right plot). The contour levels from the experiment and the simulation are the same, with $|\langle u'v' \rangle|_{\min} = 0.03$ and $\Delta\langle u'v' \rangle = 0.01$. The simulation has correctly captured the four distinct "lobes" in the Reynolds stress distribution which are antisymmetric with respect to the centerline. Evidently, the computed Reynolds stress is in agreement with the PIV experimental data.

4.2. *Turbulent flow past an oscillating cylinder at* $\mathrm{Re} = 10\,000$

In this section we examine turbulent flows past a rigid circular cylinder that undergoes a forced sinusoidal oscillation in the cross-flow direction at $\mathrm{Re} = 10\,000$; see Eq. (1). Emphasis is placed on the discussion of the influence of the cylinder oscillation on the physical quantities, and the comparison between simulation results and the experimental data by Gopalkrishnan (1993) at the same Reynolds number.

Gopalkrishnan (1993) demonstrates that the force coefficients experience a sharp increase around a certain oscillation frequency (close to the Strouhal frequency, between 0.17 and 0.18). In our simulations we have considered four oscillation frequencies, spanning from $f_0 = 0.14$ to 0.25, with a moderate displacement amplitude, $Y_0/D = 0.3$, where Y_0 is the amplitude of cylinder displacement; see Table 3 for the parameters. This range covers the frequency under which dramatic changes in drag and lift forces are observed (Gopalkrishnan, 1993). The simulations were conducted with the same resolution as in case DNS-B2.

In Fig. 6 we plot (a) the drag coefficients and (b) lift coefficient magnitudes as a function of the nondimensional frequency $f_0 D/U_0$ (where f_0 is the cylinder oscillation frequency) from the experiment (Gopalkrishnan, 1993) and from current simulations, both at $\mathrm{Re} = 10\,000$. The simulation has correctly captured the sharp rise of the force coefficients around the crucial frequency. However, it under-predicts the drag coefficients and over-predicts the lift coefficients slightly. Overall, the agreement between the simulation results and Gopalkrishnan's (1993) measurements is reasonably good. In the range of frequencies simulated, while the overall change in the drag coefficient is only moderate, the lift coefficient increases dramatically as the oscillation frequency increases.

The lift force phase angle, the angle by which the lift force leads the imposed cylinder motion, and the lift coefficient in phase with the cylinder velocity are important physical quantities as they determine the direction and the magnitude of the power transfer between the cylinder and the fluid, respectively. In Fig. 7(a) we plot a temporal window of the history of the lift coefficient and the cylinder displacement at an oscillation frequency $f_0 D/U_0 = 0.21$. It is observed that the lift force oscillates with a magnitude of about 1.6 and at the cylinder oscillation frequency. The lift signal slightly lags behind the cylinder displacement signal. The phase angle between these two signals is computed using

Table 3
Simulated cases of the flow past an oscillating cylinder

Cases	Y_0/D	$f_0 D/U_0$
$M1$	0.3	0.14
$M2$	0.3	0.17
$M3$	0.3	0.21
$M4$	0.3	0.25

Y_0 and f_0 denote the cylinder displacement amplitude and oscillation frequency, respectively.

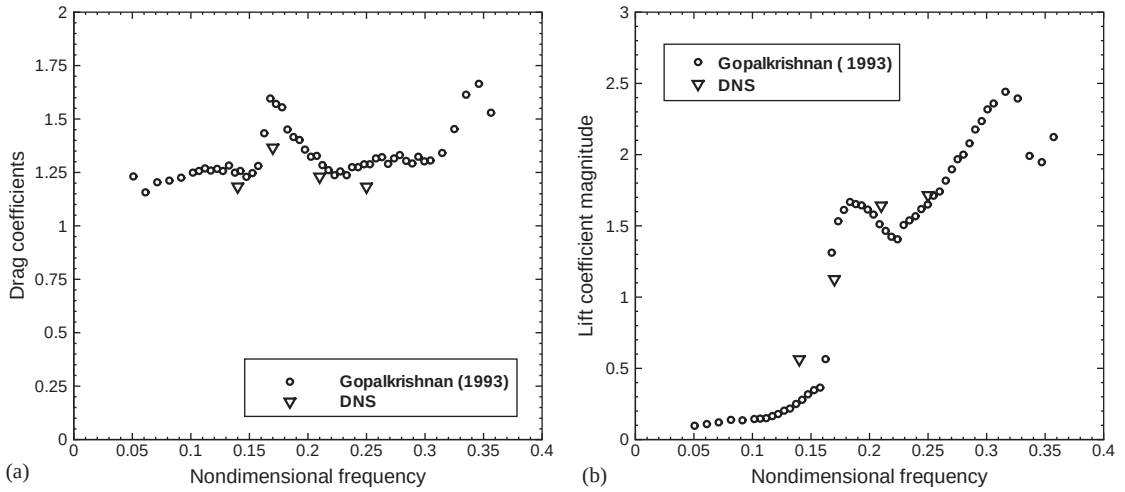

Fig. 6. (a) Drag coefficients and (b) lift coefficient magnitudes as a function of nondimensional frequency; sinusoidal oscillations; $Y_0/D = 0.3$.

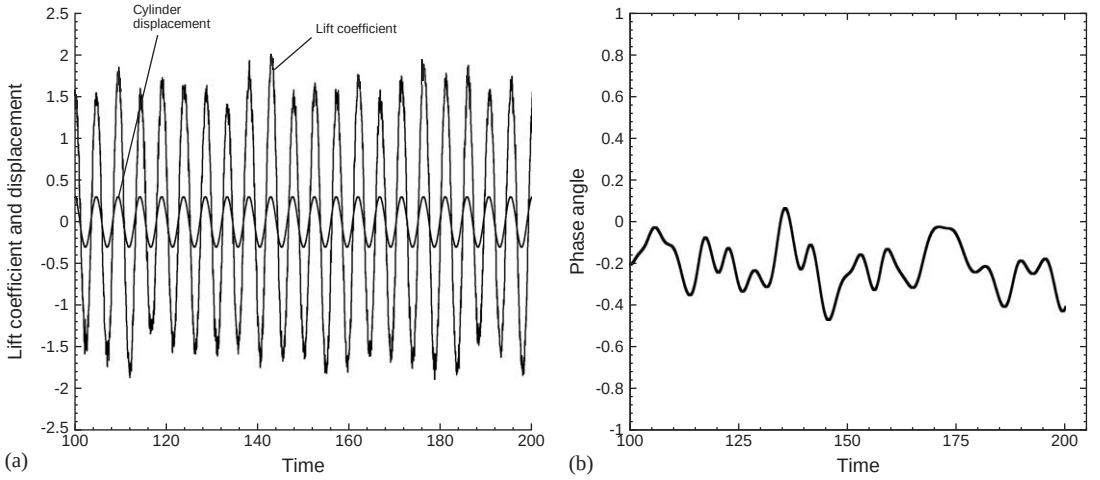

Fig. 7. (a) Time history of lift coefficient and cylinder displacement in flow past an oscillating cylinder at $\mathrm{Re} = 10\,000$; oscillation frequency $f_0 D/U_0 = 0.21$; $Y_0/D = 0.3$. (b) Time trace of the phase angle (in radians) between lift and cylinder displacement from complex demodulation analysis corresponding to the temporal window in (a).

complex demodulation analysis, and the result is shown in Fig. 7(b). The lift force phase angle varies around a mean value of -0.2 (in radians). The lift force phase angles and the lift coefficients in phase with cylinder velocity at this and the other frequencies simulated are shown in Fig. 8, together with the experimental data by Gopalkrishnan (1993). It is evident that the simulation has captured these physical quantities quite accurately.

5. Summary

We have presented the first results of direct numerical simulations of the turbulent flow past a stationary cylinder as well as past a cylinder undergoing forced harmonic oscillations at Reynolds number $\mathrm{Re} = 10\,000$. This is about an order of magnitude increase in Reynolds number from what was previously achieved. We have employed an efficient multilevel-type parallel algorithm within the spectral/*hp* element framework to tackle the computational cost.

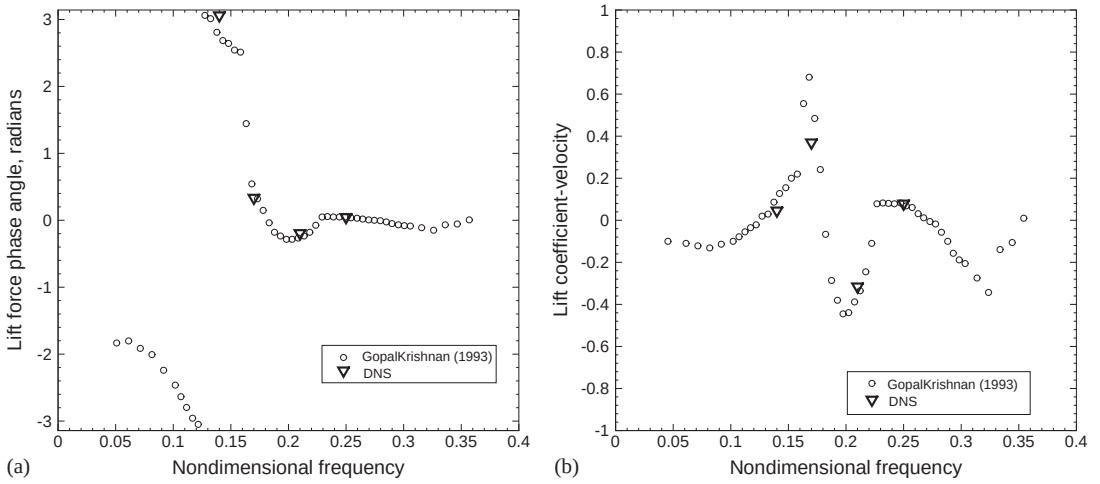

Fig. 8. (a) Phase angle between lift force and cylinder displacement and (b) the lift coefficient in phase with velocity as a function of nondimensional frequency; sinusoidal oscillations; $Y_0/D = 0.3$.

Comparisons with the available experimental data for the stationary-cylinder case show that the simulation has captured the flow quantities (including the drag, lift and base pressure coefficients and the Strouhal number) accurately, and captured the flow statistics correctly. Comparisons with the experimental data for the forced oscillation case indicate that the simulation has captured the physical quantities, such as the drag and lift coefficients, lift force phase angles, and the lift coefficients in phase with velocity reasonably well. This preliminary study demonstrates that high order based DNS is an effective tool for studying the VIV phenomena at close to realistic values of Reynolds numbers.

Acknowledgements

This work was supported by ONR. Computer time was provided by DoD's HPCMP (ARSC, NAVO. ERDC) and NSF's SDSC/PSC. We would like to thank Professor M. Triantafyllou and Professor D. Rockwell for providing the experimental data.

References

Al-Jamal, H., Dalton, C., 2004. Vortex induced vibrations using large eddy simulation at moderate Reynolds number. Journal of Fluids and Structures 19, 73–92.

Batcho, P., Karniadakis, G.E., 1991. Chaotic transport in two- and three-dimensional flow past a cylinder. Physics of Fluids A 3, 1051–1062.

Beaudan, P., Moin, P., 1994. Numerical experiments on the flow past a circular cylinder at sub-critical Reynolds number. Report TF-62, Department of Mechanical Engineering, Stanford University, USA.

Bishop, R.E.D., Hassan, A.Y., 1964. The lift and drag forces on a circular cylinder in a flowing fluid. Proceedings of Royal Society London A 277, 32–50.

Blackburn, H.M., Henderson, R.D., 1999. A study of two-dimensional flow past an oscillating cylinder. Journal of Fluid Mechanics 385, 255–286.

Blackburn, H.M., Govardhan, R.N., Williamson, C.H.K., 2000. A complementary numerical and physical investigation of vortex-induced vibration. Journal of Fluids and Structures 15, 481–488.

Braza, M., Chassaing, P., Minh, H.H., 1986. Numerical study and physical analysis of the pressure and velocity fields in the near wake of a circular cylinder. Journal of Fluid Mechanics 165, 79–120.

Braza, M., Chassaing, P., Minh, H.H., 1990. Prediction of large-scale transition features in the wake of a circular cylinder. Physics of Fluids A 2, 1461–1471.

Breuer, M., 1998. Numerical and modeling influences on large eddy simulations for the flow past a circular cylinder. International Journal of Heat and Fluid Flow 19, 512–521.

Breuer, M., 2000. A challenging test case for large eddy simulation: high Reynolds number circular cylinder flow. International Journal of Heat and Fluid Flow 21, 648–654.

Catalano, P., Wang, M., Iaccarino, G., Moin, P., 2003. Numerical simulation of the flow around a circular cylinder at high Reynolds numbers. International Journal of Heat and Fluid Flow 24, 463–469.

Dong, S., Karniadakis, G.E., 2004a. Dual-level parallelism for high-order CFD methods. Parallel Computing 30, 1–20.

Dong, S., Karniadakis, G.E., 2004b. Multilevel parallelization models in CFD. Journal of Aerospace Computing, Information and Communication 1, 256–268.

Evangelinos, C., Karniadakis, G.E., 1999. Dynamics and flow structures in the turbulent wake of rigid and flexible cylinders subject to vortex-induced vibrations. Journal of Fluid Mechanics 400, 91–124.

Evangelinos, C., Lucor, D., Karniadakis, G.E., 2000. DNS-derived force distribution on flexible cylinders subject to vortex-induced vibration. Journal of Fluids and Structures 14, 429–440.

Franke, J., Frank, W., 2002. Large eddy simulation of the flow past a circular cylinder at $Re_D = 3900$. Journal of Wind Engineering and Industrial Aerodynamics 90, 1191–1206.

Gopalkrishnan, R., 1993. Vortex-induced forces on oscillating bluff cylinders. Ph.D. Thesis, Department of Ocean Engineering, MIT, Cambridge, MA, USA.

Henderson, R.D., 1997. Nonlinear dynamics and pattern formation in turbulent wake transition. Journal of Fluid Mechanics 352, 65–112.

Jordan, S.A., 2002. Investigation of the cylinder separated shear-layer physics by large-eddy simulation. International Journal of Heat and Fluid Flow 23, 1–12.

Jordan, S.A., 2003. Resolving turbulent wakes. ASME Journal of Fluids Engineering 125, 823–834.

Kalro, V., Tezduyar, T., 1997. Parallel 3D computation of unsteady flows around circular cylinders. Parallel Computing 23, 1235–1248.

Karniadakis, G.E., Sherwin, S.J., 1999. Spectral/hp Element Methods for CFD. Oxford University Press, Oxford.

Karniadakis, G.E., Israeli, M., Orszag, S.A., 1991. High-order splitting methods for the incompressible Navier–Stokes equations. Journal of Computational Physics 97, 414–443.

Karypis, G., Kumar, V., 1998. A fast and high quality multilevel scheme for partitioning irregular graphs. SIAM Journal of Scientific Computing 20, 359–392.

Kravchenko, A.G., Moin, P., 1998. B-spline methods and zonal grids for numerical simulations of turbulent flows. Report TF-73, Department of Mechanical Engineering, Stanford University, USA.

Kravchenko, A.G., Moin, P., 2000. Numerical studies of flow over a circular cylinder at $Re_D = 3900$. Physics of Fluids 12, 403–417.

Lu, X.-Y., Dalton, C., 1996. Calculation of the timing of vortex formation from an oscillating cylinder. Journal of Fluids and Structures 10, 527–541.

Lucor, D., Imas, L., Karniadakis, G.E., 2001. Vortex dislocations and force distribution of long flexible cylinders subjected to shear flows. Journal of Fluids and Structures 15, 641–650.

Ma, X., Karamanos, G.-S., Karniadakis, G.E., 2000. Dynamics and low-dimensionality of a turbulent near wake. Journal of Fluid Mechanics 410, 29–65.

Mittal, R., Balachandar, S., 1995. Effect of three-dimensionality on the lift and drag of nominally two-dimensional cylinders. Physics of Fluids 7, 1841–1865.

Mittal, R., Moin, P., 1997. Suitability of upwind-biased finite-difference schemes for large-eddy simulation of turbulent flows. AIAA Journal 35, 1415–1417.

Mittal, S., Kumar, V., 2001. Flow-induced vibrations of a light circular cylinder at Reynolds numbers 10^3 to 10^4. Journal of Sound and Vibrations 245, 923–946.

Moeller, M.J., Leehey, P., 1984. Unsteady forces on a cylinder in cross flow at subcritical Reynolds numbers. In: Paidoussis, M.P., Griffin, O.M., Sevik, M. (Eds.), ASME Symposium on Flow-Induced Vibrations, vol. 1. New Orleans, ASME, New York, pp. 57–71.

Newman, D.J., Karniadakis, G.E., 1997. A direct numerical simulation study of flow past a freely vibrating cable. Journal of Fluid Mechanics 344, 95–136.

Norberg, C., 1992. Pressure forces on a circular cylinder in cross flow. In: Eckelmann, et al. (Eds.), Proceedings of IUTAM Conference on Bluff Body Wake Instabilities. Springer, Berlin.

Norberg, C., 2003. Fluctuating lift on a circular cylinder: review and new measurements. Journal of Fluids and Structures 17, 57–96.

Prasad, A., Williamson, C.H.K., 1997. The instability of the shear layer separating from a bluff body. Journal of Fluid Mechanics 333, 375–402.

Saelim, N., Rockwell, D., 2003. Near-wake of a cylinder in the range of shear layer transition. Physics of Fluids, submitted for publication.

Sarpkaya, T., 2004. A critical review of the intrinsic nature of vortex-induced vibrations. Journal of Fluids and Structures 19, 389–447.

Skaugset, K.B., Larson, C.M., 2003. Direct numerical simulation and experimental investigation on suppression of vortex induced vibrations of circular cylinders by radial water jets. Flow, Turbulence and Combustion 71, 35–59.

Szepessy, S., Bearman, P.W., 1992. Aspect ratio and end plate effects on vortex shedding from a circular cylinder. Journal of Fluid Mechanics 234, 191–217.

Travin, A., Shur, M., Strelets, M., Spalart, P., 1999. Detached-eddy simulations past a circular cylinder. Flow, Turbulence and Combustion 63, 293–313.

Triantafyllou, M.S., Hover, F.S., Techet, A.H., 2004. Reynolds number effect on VIV: from subcritical to supercritical flow. In: E. de Langre, F. Axisa (Eds.), Proceedings of the Eighth International Conference on Flow-Induced Vibration, Paris, France, p. 21.

Tutar, M., Holdo, A., 2000. Large eddy simulation of a smooth circular cylinder oscillating normal to a uniform flow. ASME Journal of Fluids Engineering 122, 694–702.

Unal, M.F., Rockwell, D., 1988. On vortex shedding from a cylinder: Part I, the initial instability. Journal of Fluid Mechanics 45, 203.

West, G.S., Apelt, C.J., 1993. Measurements of fluctuating pressures and forces on a circular cylinder in the Reynolds number range 10^4 to 2.5×10^5. Journal of Fluids and Structures 7, 227–244.

Wieselsberger, C., 1921. Neuere Feststellungen uber die Gesetze des Flussigkeits und Luftwiderstands. Physikalische Zeitschrift 22, 321–328.

Willden, R.J., Graham, J.M.R., 2004. Multi-modal vortex-induced vibrations of a vertical riser pipe subject to a uniform current profile. European Journal of Mechanics B 23, 209–218.

Williamson, C.H.K., 1996. Vortex dynamics in the cylinder wake. Annual Review of Fluid Mechanics 28, 477–539.

Williamson, C.H.K., Govardhan, R., 2004. Vortex-induced vibrations. Annual Review of Fluid Mechanics 36, 413–455.

Zhang, J., Dalton, C., 1996. Interactions of vortex-induced vibrations of a circular cylinder and a steady approach flow at a Reynolds number of 13 000. Computers and Fluids 25, 283–294.